Ground-Motion Models for Very-Hard-Rock Sites in Eastern North America: An Update

by David M. Boore

ABSTRACT

The ground-motion models provided by me to the Next Generation Attenuation-East (NGA-East) project in 2015 have been updated by considering three additional Fourier spectra attenuation models and by conducting a mixed-effect analysis of the residuals between the ground-motion intensity measures computed from the attenuation models and the data from nine relatively well-recorded events in eastern North America. On the basis of the period trends of the bias in the residuals and the distance trends of the residuals, I recommend the ground-motion models developed for these attenuation models, with equal weights: the BCA10D model with $1/R$ geometrical spreading at all distances, and two modifications of the Atkinson and Boore (2014; referred as AB14) model, with $1/R$ spreading within 10 km, $1/R^{1.3}$spreading from 10 to 50 km, and $1/\sqrt{R}$ spreading beyond 50 km.

Electronic Supplement: Residual figures for ground-motion models (GMMs), and zip files containing the BCA10D, AB14mod1, and AB14mod2 GMMs and the parameter files and random-vibration adjustment files used in the stochastic model simulations.

INTRODUCTION

In the Next Generation Attenuation-East (NGA-East) project (Goulet *et al.*, 2015), I was asked to provide potential ground-motion "seed" models (GMMs) corresponding to six attenuation models provided by the Project Team (Atkinson *et al.*, 2015). Seed models are used to derive a set of median GMMs that span the model space, as discussed by Goulet *et al.* (2017). The attenuation models specify the geometric spreading and anelastic attenuation (as specified by the $Q(f)$ function) of Fourier amplitude spectra. To do this, I first obtained stress parameters for each attenuation model by inverting pseudoacceleration response spectra (PSA) data at 0.1 and 0.2 s from nine of the best-recorded earthquakes in eastern North America (ENA) with magnitudes greater than 4.4, following the procedure described in Boore *et al.* (2010) and Boore (2012); the events are listed in Table 1. The stress parameter plays a key role in determining high-frequency motions from earthquakes, as discussed in Boore (2003). The stress parameters obtained from the data inversions were used to derive the GMMs, one for each attenuation model, using the stochastic method as implemented in the Stochastic-Method SIMulation (SMSIM) programs of Boore (2005). The results were reported in Boore (2015; hereafter, B15). In B15, the ground motions for several periods (0.1, 0.2, 1.0, and 2.0 s) were compared with data from the nine earthquakes, and it was noted that several models were in poor agreement with the longer-period data. These longer-period data are not sensitive to the stress parameter and therefore were not used in the inversions for those parameters. The intent of using all of the seed models, even if they did not agree with the longer-period data, was to "make sure that a minimum range of models representing the epistemic uncertainty in attenuation, as represented by the literature, would be made available to the Project Team" (Goulet *et al.*, 2017, p. 41). Although all six GMMs were accepted as seed models by the NGA-East project (Goulet *et al.*, 2017), I do not endorse all of the models for individual use. Here is what I said on p. 48 of B15: "Even though I show that the models with $1/R^{1.3}$geometrical spreading cannot fit longer-period data, no matter what stress parameter is used, I provide motions for those models anyway. Although I am not endorsing any one model, if I had to choose one, it would be the BS11 model. If I were allowed to choose three, they would be AB95, BCA10D, and BS11." (The models and their names are described in the footnote to Table 2). In this article, I revisit those conclusions, and now recommend three models that fit a range of data but have very different attenuation rates in the data-poor region less than 50 km. One model is the BCA10D model, for which the attenuation due to geometrical spreading (with no anelastic attenuation) is $1/R$ for all distances, and the other two are modifications of the Atkinson and Boore (2014; hereafter, AB14) model, with $1/R$ spreading within 10 km and $1/R^{1.3}$ spreading between 10 and 50 km, followed by $1/\sqrt{R}$ spreading at greater distances.

The emphasis in this article is on the GMMs, not on the determination of the stress parameters used to derive those models and the accompanying correlation between the attenuation models and the stress parameters. Those items are discussed more fully in Boore *et al.* (2010), Boore (2012), and B15.

doi: 10.1785/0220170218

Table 1
Events Used to Determine Stress Parameters and in the Residual Analysis

Event	Date (yyyy/mm/dd)	Epicentral Latitude (°N)*	Epicentral Longitude (°E)*	NGA-East M
Nahanni	1985/12/23	62.187	−124.243	6.76
Saguenay	1988/11/25	48.117	−71.184	5.85
Mt. Laurier	1990/10/19	46.474	−75.591	4.47
Cap Rouge	1997/11/06	46.801	−71.424	4.45
St. Anne†	1999/03/16	49.615	−66.344	4.43
Kipawa	2000/01/01	46.840	−78.925	4.62
Ausable Forks	2002/04/20	44.513	−73.699	4.99
Riviere-du-Loup	2005/03/06	47.753	−69.732	4.65
Val des Bois	2010/06/23	45.904	−75.497	5.10

*From the Next Generation Attenuation-East (NGA-East) flatfile.
†Called CoteNord in the NGA-East flatfile.

MODEL DEVELOPMENT

In this study I used nine attenuation models, as briefly described in Table 2 (the model names are explained in the footnote to the table). Included were the six models used by B15, as well as the A04QL model used by Boore (2012); this model was first proposed by Atkinson and Assatourians (2010). This model is the same as A04TL (referred to as "A04" in B15), except it decays as $1/R$ rather than $1/R^{1.3}$ within 10 km. The advantage of the A04QL model is that it has a $1/R^{1.3}$ decay from 10 to 50 km, which is consistent with studies of small events (e.g., Atkinson, 2004), but it does a better job of matching the longer-period data than the A04TL model, which has $1/R^{1.3}$ decay for all distances less than 50 km, not just beyond 10 km. After studying some preliminary results, I added two models that are similar to A04QL within 50 km but change to $1/\sqrt{R}$ decay at 50 km, with no transition distance as in the A04QL model. It was noted in Boore *et al.* (2010) that the presence or absence of a transition distance can have an important impact on the prediction of ground motions of

Table 2
Median Stress Parameters from Inversion of Pseudoacceleration Response Spectra (PSA) Values for $T = 0.1$ and 0.2 s for Nine Earthquakes

Model	Description*	$\Delta\sigma_{200}$ (bars)†	$\Delta\sigma_{600}$ (bars)†	$\Delta\sigma_{200}/\Delta\sigma_{600}$‡
A04QL	−1.0(10)−1.3(70)0.2(140)−0.5	338	99	3.4
A04TL	−1.3(70)0.2(140)−0.5	1659	301	5.5
AB14	−1.3(50)−0.5 (modified for periods > 0.2 s)	1792	879	2.0
AB14mod1, AB14mod2§	−1.0(10)−1.3(50)−0.5	358	229	1.6
AB95	−1.0(70)0.0(130)−0.5	147	70	2.1
BCA10D	−1.0	193	122	1.6
BS11	−1.0(50)−0.5	206	173	1.2
SGD02	−1.1(80)−0.55	462	185	2.5

*The entries are shorthand for the geometrical spreading function; the numbers in parenthesis are the breakpoint distances, with the exponent of R being given by the numbers on either side of the breakpoint distance. The sources of the models are as follows: A04QL is the modification of the Atkinson (2004) model (A04TL) introduced by Atkinson and Assatourians (2010); QL, quadrilinear; and TL, trilinear. AB14, AB95, BCA10D, BS11, and SGD02 are from Atkinson and Boore (2014), Atkinson and Boore (1995), Boore *et al.* (2010), Boatwright and Seekins (2011), and Silva *et al.* (2002), respectively. AB14mod1 and AB14mod2 are described in the first paragraph of the Model Development section. The Q models for all but AB14mod1 and AB14mod2 are given in table 2.1 of Boore (2015). The Q models for AB14mod1 and AB14mod2 are the same as that for the AB14 model.
†$\Delta\sigma_{200}$ and $\Delta\sigma_{600}$: stress parameters from inversions of PSA from data recorded at distances $R_{RUP} \le 200$ km and $R_{RUP} \le 600$ km, respectively.
‡Ratio of the $\Delta\sigma_{200}$ and $\Delta\sigma_{600}$ stresses (an indication of how well the attenuation model fits the data for a wide range of distances).
§The stress parameters are the same for AB14mod1 and AB14mod2.

engineering interest. The first new model is a modification of AB14, replacing the $1/R^{1.3}$ geometrical spreading within 10 km with $1/R$ spreading but retaining the frequency-dependent geometrical spreading of AB14 (which applies at distances less than 50 km and $f < 5$ Hz). This model is termed AB14-mod1. The second new model is a simplification of AB14-mod1, in which the frequency-dependent adjustment given by equations (6) and (7) of Atkinson and Boore (2014) is not applied (i.e., $T_C C_{LF} = 0.0$ in equation 9 of AB14); this model is denoted as AB14mod2. Although the Fourier acceleration spectra for the AB14mod1 and AB14mod2 models are identical for $f \geq 5$ Hz, the response spectra derived from these models can differ at frequencies greater than 5 Hz, as will be shown later.

The average attenuation behavior captured by the models used in this article is a result of a complex interaction of wave propagation, source radiation pattern, and source directivity effects (e.g., Chapman and Godbee, 2012; Frankel, 2015). The faster than $1/R$ attenuation at distances between about 10 to at least 50 km is supported by a number of observational studies (e.g., Atkinson, 2004; Atkinson and Boore, 2014; Wu *et al.*, 2016), although the rate of geometrical spreading has been found to be a function of frequency in some studies (e.g., Frankel, 2015, found −1.5 at 1 Hz and −0.8 at 14 Hz), and some studies (e.g., Sedaghati and Pezeshk, 2016) find frequency-dependent geometrical spreading near $1/R$. In addition, simulation studies find faster than $1/R$ geometrical spreading out to at least 50 km (e.g., Chapman and Godbee, 2012, and Frankel, 2015, for 1 Hz). The observational studies have little to say about the rate of attenuation as a function of R_{RUP} within 10 km, given that most of the small-to-moderate-sized events used in those studies have focal depths near or exceeding 10 km. I do note, however, that the simulations by Chapman and Godbee (2012) show an increase of motion within 10 km, due presumably to radiation pattern effects. This and the fact that rays will largely be traveling upward for sites at small epicentral distances, with correspondingly less interaction of multiple wave arrivals, suggests that $1/R$ behavior for small distances is not unreasonable. Because the stress parameters are determined by extrapolating fits to data at greater distances to an effective distance of 1 km, using $1/R$ geometrical spreading within 10 km leads to much lower stress parameters than if $1/R^{1.3}$ is used all the way to the source, as is shown by the results discussed in the next paragraph.

Inversions for the stress parameters used in the stochastic method simulations were made for the nine attenuation models. For each model, the stress parameters were inverted for two categories: data recorded at distances less than 200 km and less than 600 km (as in B15), resulting in 18 average stress parameters. For convenience, I refer to the stress parameters from data within 200 km and within 600 km as $\Delta\sigma_{200}$ and $\Delta\sigma_{600}$, respectively. The stochastic-model parameters other than the geometric spreading and Q function (e.g., path-dependent duration, average radiation pattern, and site amplification) were the same as used in B15. The data used are for hard-rock sites in ENA, as discussed by Boore *et al.* (2010) and Boore (2012).

For each attenuation model and distance cutoff, a stress parameter was found for each of the nine events. Comparisons of simulated and observed motions are shown in Boore (2012, 2015) for selected events and attenuation models; the comparisons for the current results are similar and are not shown in order to save space. These stress parameters are shown in Figure 1. In general, the stress parameters from the two largest events bound those from the other seven events; in addition, they seem to be outliers for a number of the attenuation models, being factors of 2 or more smaller and larger than the range of stress parameters from the other events. Although it is difficult to be certain with only a small number of events, the distribution of log stress parameter for the other seven events seems to be more uniform than normal. For these reasons, the average stress parameter used in the simulations for the GMM was the median of the nine event stresses, rather than the geometric mean stress as in B15. The stress parameter for the Saguenay earthquakes was excluded in B15, but it is now included. The median stresses $\Delta\sigma_{200}$ and $\Delta\sigma_{600}$ are given in Table 2 and are plotted in Figure 1; note that the stress parameters for the models with $1/R^{1.3}$ decay to the source are significantly higher than for the other models. In deriving the stress parameters, I also used the magnitudes for each event given in the NGA-East flatfile (see Data and Resources) in the inversions for the stress parameters, rather than those used in B15, as discussed later. The ratios of $\Delta\sigma_{200}$ and $\Delta\sigma_{600}$ are given in the last column of Table 2. The median stresses $\Delta\sigma_{200}$ and $\Delta\sigma_{600}$ are very similar for the BS11 attenuation model (Fig. 1b), with the next best comparison being for the BCA10D and the AB14mod models (Fig. 1a and 1g, respectively).

RECOMMENDED GMMS

For each of the average stress parameters, I simulated ground motions for the magnitudes and distances of the data for each event used in the inversions. I used the program *tmrsk_loop_rv_drvr* in the SMSIM suite of programs (see Data and Resources); the parameter files are included in the Ⓔ electronic supplement to this article. These are the candidate GMMs, evaluated at the magnitudes and distances of the data. For general use, the GMMs are specified by tables of ground motions for many magnitudes and distances, one table for each period. A mixed-effect analysis was performed of the residuals $(R_{ij})_k$ between the observed and the simulated motions, using this equation, modified from Scasserra *et al.* (2009):

$$(R_{ij})_k \equiv \log(O_{ij}/P_{ij})_k = c_k + (\eta_i)_k + (\varepsilon_{ij})_k, \qquad (1)$$

in which O_{ij} and P_{ij} are the observed and predicted motions for event i at station j, respectively; log is the common (base 10) logarithm; and c_k is a fixed effect representing the mean bias in the residuals for the attenuation model/$\Delta\sigma$ combination designated by k, after removing the random-effect event terms η_i. The event terms and the within-event residuals ε_{ij} have zero means. Graphs of the within-event (ϕ), between-event (τ), and total (σ) standard deviations from the mixed-effects analysis are

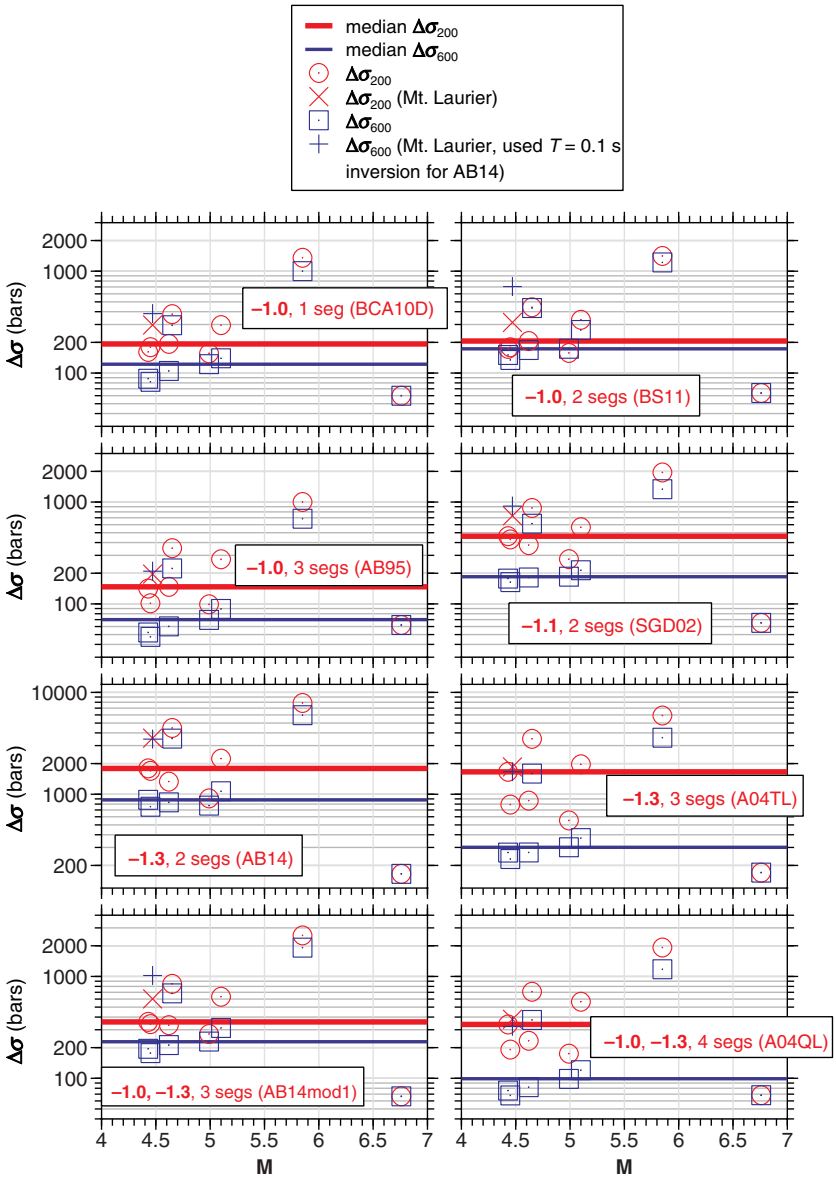

▲ **Figure 1.** Stress parameters for individual events (symbols) and average stress parameters (the medians of the individual stress parameters) (lines) for eight attenuation models and the two distance limits (the results for AB14mod2 are not shown because they are almost identical to those from AB14mod1). The powers of distance for the attenuation functions within 50 km and the number of segments (segs) are given in the comment in each graph (see Table 2 for more details). The graphs are arranged by model complexity, the simplest at the top. The color version of this figure is available only in the electronic edition.

shown in Figure 2. The figure also shows the same quantities for the global ergodic model of Al Atik (2015), derived from many more data than used in this article for two magnitudes that approximately bound the data used here. Recalling that most data used in the analysis for this article come from events with magnitudes between 4 and 5, I show Al Atik's results for **M** 4.5 (and **M** 6.5, near the magnitude of the largest event used in this article). The uncertainties from the limited data set used in the inversions for stress parameters are similar to those from the much larger data sets used by Al Atik (2015) for most of the attenuation models, suggesting that the data used for the stress parameter inversions are a representative sample of ENA data.

Although there are formal quantitative methods for selecting and ranking GMMs (e.g., Scherbaum *et al.*, 2009; Kale and Akkar, 2013; Mak *et al.*, 2017), in view of the limited number of events and data, I prefer to choose the GMMs based on a subjective evaluation of the 18 GMMs (9 attenuation models and 2 stresses per model, for the maximum distances of 200 and 600 km). I used plots of the bias and the residuals to make the subjective evaluations. Bias plots are given in Figure 3. All data for the nine events recorded at distances within 2000 km were used in the analysis, although the stress parameters used for the GMMs were determined from inversions of 0.1 and 0.2 s PSA within 200 and 600 km. A residual analysis using data only within 800 km gave similar results. The bias terms for some attenuation models have a pronounced dependence on period (e.g., SGD02), whereas A04QL has little period dependence but a large nonzero bias for the GMM using the stress determined using data within 200 km. The simplest $1/R$ model BCA10D and the modified $1/R^{1.3}$ models AB14mod1 and AB14mod2 have little period dependence and small overall biases for both the $\Delta\sigma_{200}$ and the $\Delta\sigma_{600}$ stresses. For these three attenuation models, the biases for the $\Delta\sigma_{200}$ stress are somewhat closer to 0.0 than for the $\Delta\sigma_{600}$ stress. On the basis of the small overall bias and little period dependence, I tentatively identified the two AB14mod models and the BCA10D model, for $\Delta\sigma_{200}$, as being those that I would recommend for general use. As mentioned earlier, in B15 I had also recommended AB95 and BS11 GMMs, but based on the trends of the bias with period for BS11 and the negative bias for AB95, I no longer do so.

Plots of the residuals versus distance for several periods are another basis for choosing the models. The usual practice is to plot the within-event residuals versus some predictor variable to look for trends suggesting modifications needed in the predicted motions. The within-event residuals have had the overall bias and the between-event terms removed, as indicated in the following equation:

$$(\varepsilon_{ij})_k = (R_{ij})_k - (\eta_i)_k - c_k. \quad (2)$$

For purposes of making a judgment about the various GMMs, however, I found it more meaningful to make plots of the

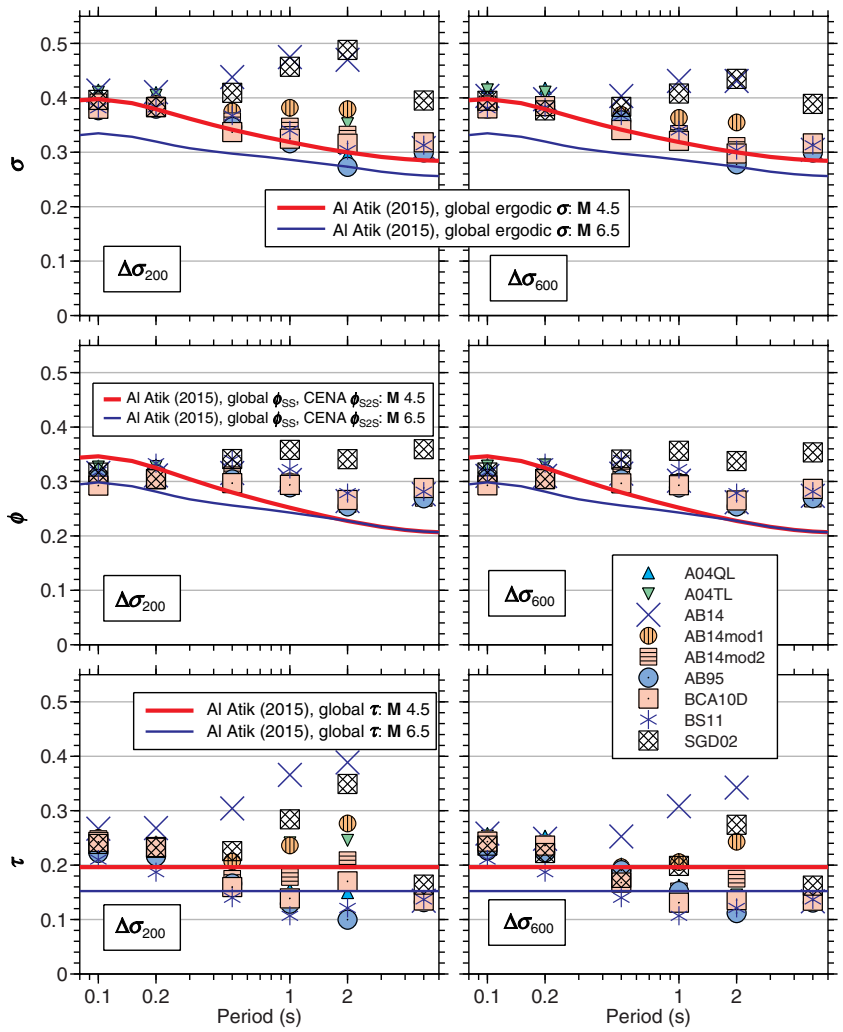

▲ **Figure 2.** Within-event (ϕ), between-event (τ), and combined ($\sigma = \sqrt{\phi^2 + \tau^2}$) uncertainties from the mixed-effects analysis of the residuals computed between the data and the simulated motions using the indicated attenuation models and stress parameters. ϕ and τ are the standard deviations (base10) of ε_{ij} and η_i in equation (1), respectively. The color version of this figure is available only in the electronic edition.

residuals after adding back the overall bias, because this is more representative of the agreement between the observations and the predictions for a given GMM. Figures 4 and 5 show plots of $(\varepsilon_{ij})_k + c_k$ versus R_{RUP} for periods of 0.2 and 2.0 s, respectively. Plots for other periods are given in the Ⓔ electronic supplement to this article, as are residual plots for GMMs using $\Delta\sigma_{600}$. The ordinate range for the residuals (Figs. 4 and 5) are larger than for the bias plots (Fig. 3); this can hide significant nonzero biases. For example, a cursory glance at the A04QL residuals for $T = 2$ s in Figure 5 might suggest little dependence on R_{RUP}, but Figure 3 shows a significant negative bias that is independent of period.

The choice of a GMM should not be made on the basis of the bias terms c_k or the residuals at a single period alone. For example, the residuals for the A04TL GMM for the $\Delta\sigma_{200}$ stress parameter have little dependence on R_{RUP} for $T = 2$ s (Fig. 5), but they do for $T = 0.2$ (Fig. 4), and the bias term c_k shows an obvious trend with period (Fig. 3). The residuals for the BCA10D and the AB14mod GMMs using the $\Delta\sigma_{200}$ stresses show relatively little dependence on R_{RUP} within about 700 km, and the bias terms are close to zero, with little period dependence. On this basis, the BCA10D $\Delta\sigma_{200}$ and two AB14mod $\Delta\sigma_{200}$ models are my recommendations for individual use (as opposed to the need for a number of seed models as in the NGA-East project). For brevity, these models will hereafter be referred to as the BCA10D and the AB14mod GMMs (with the modification number 1 or 2 added when needed), without specifying that the $\Delta\sigma_{200}$ stress parameter was used.

The motions from these three models are shown as a function of R_{RUP} in Figure 6, for PSA at 0.2 and 2.0 s, and a suite of magnitudes. The 2.0 s motions for all models approach one another at small distances and magnitudes, because those motions are controlled by the moment magnitude (the source corner frequencies for the smaller earthquakes being much higher than the 0.5 Hz frequency of the 2 s oscillator). Although $\Delta\sigma_{200}$ is the same for both AB14mod models (Table 2), the longer-period, larger-magnitude motions are greater for the AB14mod1 model than for the AB14mod2 model. There are two factors that combine to produce this apparent inconsistency: (1) the geometric spreading for the AB14mod1 model at frequencies less than 0.2 Hz is less rapid than for the AB14mod2 model, with the largest difference for distances between about 10 and 20 km (e.g., fig. 9 in Atkinson and Boore, 2014); and (2) the effective point-source distance used in the simulations is given by $R_{PS} = \sqrt{R_{RUP}^2 + h^2}$, in which h is a magnitude-dependent finite-fault adjustment factor given by Boore and Thompson (2015). For example, for $\mathbf{M} = 7$ and $R_{RUP} = 0$ km, the geometrical spreading for the AB14mod models is evaluated at $R_{PS} = 12.8$ km, in which the difference in the geometrical spreading in the two models is near a maximum, leading to the observed difference in predicted PSA shown in Figure 6.

A more comprehensive display of the comparison of the motions from the two AB14mod GMMs is given in Figure 7, which shows the ratios of the motions as a function of period. The period, magnitude, and distance dependence of the ratios can be assessed from the different symbols types, sizes, and colors. This figure shows that there are small differences in the motions for periods less than 0.2 s, in which the Fourier spectra are the same for both models (this is because of the nature of response spectra obtaining some of their response from ground motions at frequencies away from the oscillator

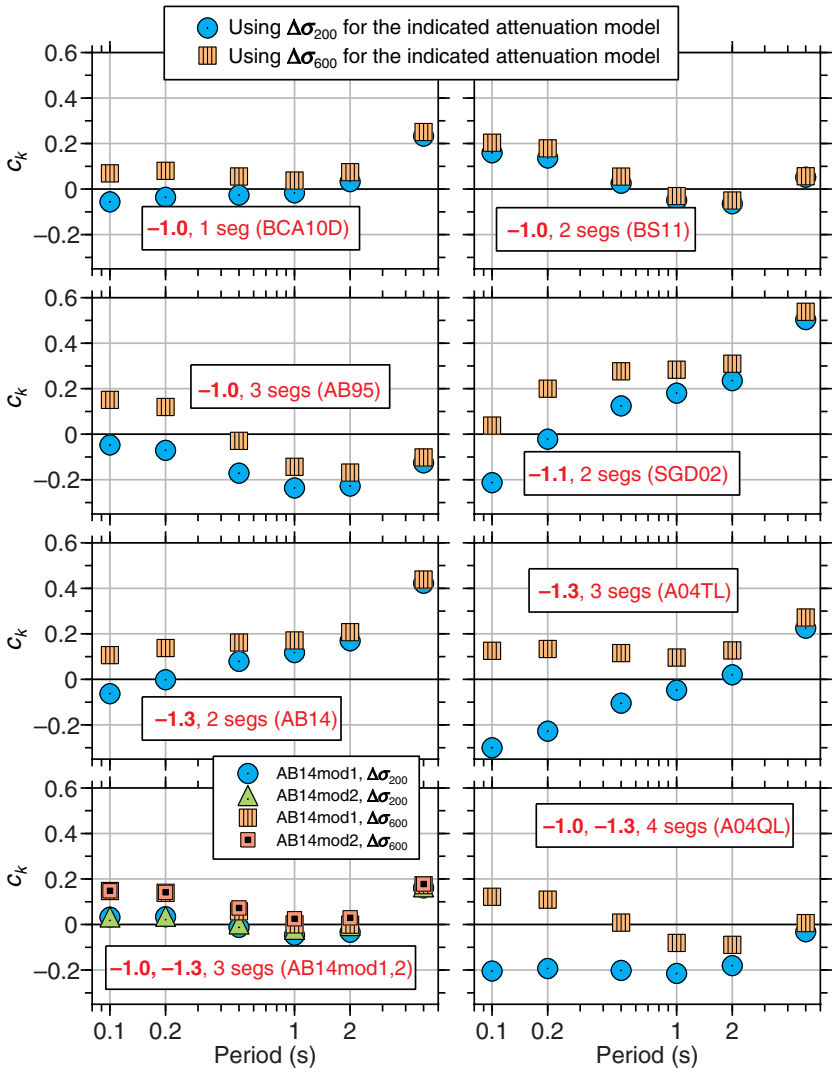

▲ **Figure 3.** Bias c_k for each attenuation model (using both $\Delta\sigma_{200}$ and $\Delta\sigma_{600}$) against period, from residuals in terms of common logarithms. The graphs are arranged by model complexity, the simplest at the top. The color version of this figure is available only in the electronic edition.

frequency). The largest differences are for longer periods, closer distances, and larger magnitudes, as already seen in Figure 6. The AB14mod2 GMM motions are smaller than the AB14mod1 GMM motions, with the maximum difference corresponding to a factor of 0.64.

DISCUSSION

Oversaturation

A careful inspection of the $T = 0.2$ s graph in Figure 6 shows that the predicted motions for smaller earthquakes can exceed those from larger earthquakes at close distances for the AB14-mod models. This is seen more clearly in Figure 8, which shows the $T = 0.1$ s motions within 20 km. This oversaturation is due to the use of the Boore and Thompson (2015) finite-fault factors used to convert the finite-fault rupture distance R_{RUP} to the equivalent point-source distance R_{PS} used in the stochastic model simulations. This oversaturation was recognized and discussed in both Boore and Thompson (2015) and B15. In the NGA-East project, a modification was applied by Youngs and Kuehn (2015) to the B15 GMMs to avoid the aesthetically unpleasing oversaturation. I have not made a similar modification to the GMM tables accompanying this article for several reasons: (1) it could be that oversaturation is physical, as residuals for large earthquakes used in the NGA-West2 projects suggest (e.g., Boore *et al.*, 2014); and (2) the oversaturation occurs for R_{RUP} within 10 km, but this implies a shallow source, and studies such as Hollenback *et al.* (2015) find that the average stress parameter should decrease with decreasing depth, with the effect being more pronounced for small than large earthquakes. This would lead to smaller motions at close distances for the smaller events; no depth adjustments were include in the GMMs in this article.

Comparison with the B15 BCA10D GMM

Figure 9 shows the ratios of the ground-motion intensity measures (GMIMs) provided to the NGA-East project (B15) and those from the GMM proposed in this article, for the BCA10D GMM. The AB14mod attenuation models were not used by B15, so a comparable comparison cannot be made. The largest differences are for short periods; for a given period, the differences increase with magnitudes. Distance has a small influence on the ratios. The behavior of the ratios is expected on the basis of the relative size of the source corner period and the oscillator period. As earthquake size increases, the source corner period will move to larger values than the GMIM period, and the GMIM will have an increasing sensitivity to the stress parameter. These stress parameters are 173 bars for the NGA-East GMM and 193 bars for the GMM proposed in this article; the ratio of the high-frequency levels of the Fourier spectra is $(173/193)^{2/3} = 0.93$; this is consistent with Figure 9. The differences in the stress parameters are largely due to differences in the magnitudes of the earthquakes used in determining the stresses, as discussed next.

Dependence of Stress on M and Median versus Geometric Mean

The stress parameter derived from inversions of PSA can be quite sensitive to the moment magnitudes of the events providing the data to be inverted. For example, Boore *et al.* (2010) found a factor of 2.6 increase in the stress parameter derived from the Riviere-du-Loup earthquake when the magnitude was changed from 5.0 (used in Atkinson and Boore, 2006) to 4.67. In this article, I use the moment magnitudes from the

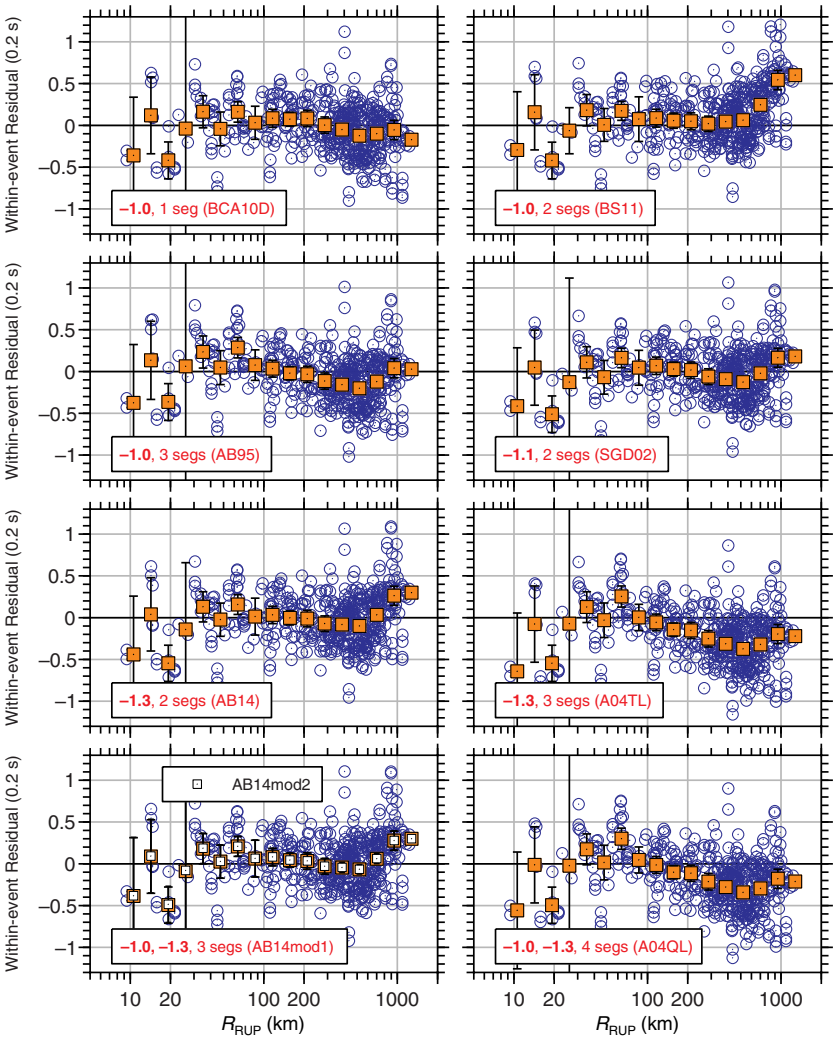

▲ **Figure 4.** Within-event residuals (base10) of $T = 0.2$ s pseudoacceleration response spectra (PSA) (circles) after adding back the overall bias c_k, as a function of distance, for each of the attenuation models (and $\Delta\sigma_{200}$). The filled squares are averages in distance bins for the models given in the boxed comments; the unfilled squares in the lower left graph are bin averages for the AB14mod2 model. The bars, barely visible for the larger distances, are 95% confidence intervals of the bin averages for the models in the legends. Note the larger range of the ordinate values than for the bias plots in Figure 3. The graphs are arranged by model complexity, the simplest at the top. The color version of this figure is available only in the electronic edition.

NGA-East flatfile (see Data and Resources); those magnitudes differ somewhat from those used in B15, as shown in Table 3. $\Delta\sigma_{200}$ for each event, as well as the median $\Delta\sigma_{200}$, is given in Table 3 for the BCA10D and the AB14mod1 attenuation models, for both sets of magnitudes. The median $\Delta\sigma_{200}$ from the B15 magnitudes is higher than from the NGA-East magnitudes for all models, by about the same ratio (1.21 for BCA10D GMM and 1.24 for the two AB14mod GMMs). The consequences of the stress parameter differences are shown in Figure 10, which shows ratios of the motions for the AB14-mod1 attenuation model and the stress parameters obtained from the different sets of magnitudes (plots for the other two models are very similar). The trends are similar to those in Figure 9, with the largest differences being at short periods and large earthquakes. The GMIMs from the simulations using the different stress parameters differ by less than 15%.

Another reason for a difference in the GMMs of B15 and in this article is the current determination of the stress parameters from the median of the individual event stress parameters, rather than the geometric mean of those stress parameters. Table 4 compares the various determinations of $\Delta\sigma_{200}$: from the two sets of magnitude and using the median and the geometric mean. In general, the two sets of magnitudes lead to larger differences in the stress parameters than does the type of average used.

In conclusion, the different sets of magnitudes and the type of average being used to determine the stress parameters used in deriving the GMMs does not contribute a large uncertainty in the GMMs. More important is the attenuation model and the epistemic uncertainty in the stress parameters due to the limited number of events and data per event; as seen in Figure 1, there is a large scatter in the stress parameters for the individual events. Some of this is probably aleatory variability in the stress parameter for each event, and some of it is due to the limited number of recordings per event. The GMMs in this article only represent the median ground motions. In applications, the aleatory uncertainty needs to be taken from studies such as Al Atik (2015).

Choosing between the BCA10D and AB14mod GMMs

It is hard to distinguish between the three models on the basis of the available data, because the biases and residuals shown in Figures 3–5 are comparable. If anything, the BCA10D short-period residuals have somewhat less of a trend with distance than do the residuals for the AB14mod models (the upper and lower graphs in the left column of Fig. 4), but the difference is primarily at longer distances for which it is not clear that the data are representative of the true trends, given the possibility of data censuring due to only the larger amplitude data being above the noise. On the other hand, the AB14mod1 attenuation model is based on the analysis of Fourier acceleration spectra from many small events (Atkinson and Boore, 2014) and thus has a better empirical basis than the other two models.

For short-period motions, the differences in the models show up most strongly at great distances, a combination of periods and distances of little or no practical application. At distances within 100 km, the differences are largest at

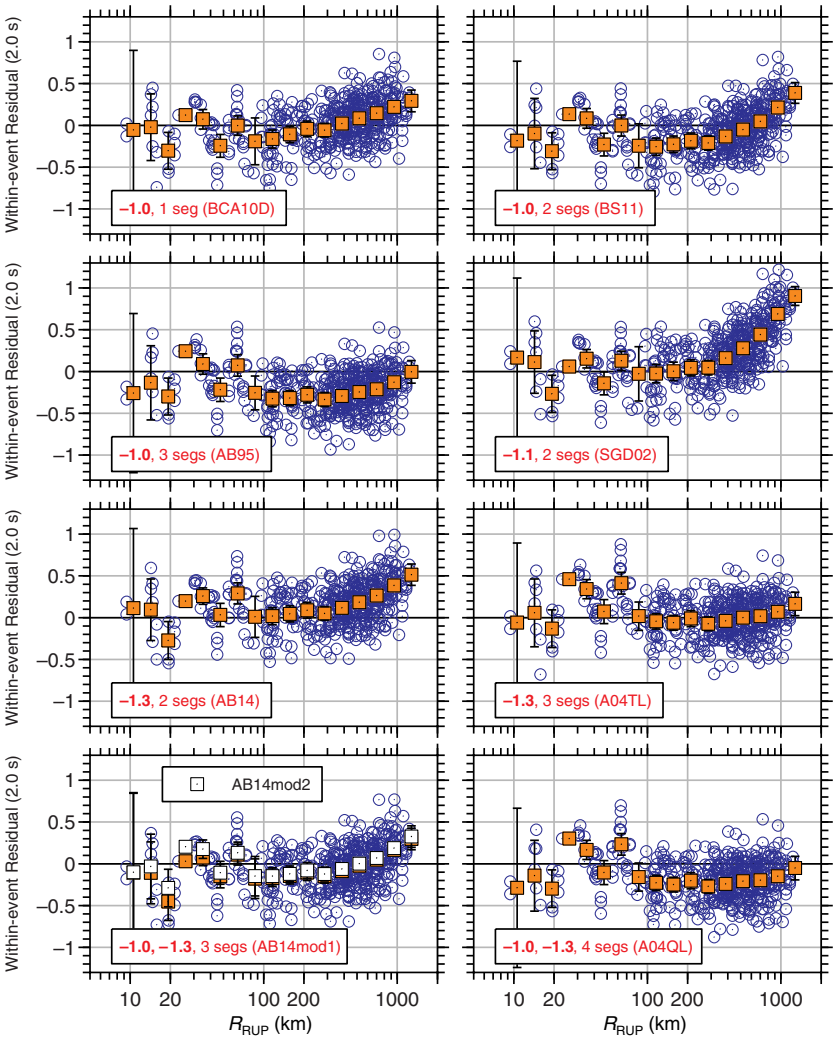

▲ **Figure 5.** Within-event residuals (base10) of $T = 2.0$ s PSA (circles) after adding back the overall bias c_k, as a function of distance, for each of the attenuation models (and $\Delta\sigma_{200}$). The filled squares are averages in distance bins for the models given in the boxed comments; the unfilled squares in the lower left graph are bin averages for the AB14mod2 model. The bars, barely visible for the larger distances, are 95% confidence intervals of the bin averages for the models in the legends. Note the larger range of the ordinate values than for the bias plots in Figure 3. The graphs are arranged by model complexity, the simplest at the top. The color version of this figure is available only in the electronic edition.

50 km, for which the AB14mod attenuation models transition from $1/R^{1.3}$ to $1/\sqrt{R}$ geometrical spreading. Even here, the largest differences are for small magnitudes, with the BCA10D GMM motions being a factor of less than 1.6 larger than the AB14mod GMM motions. Although the motions at large distance from small magnitudes and short periods are of little practical importance, that is not true of long-period motions from large-magnitude events. This combination of distance, magnitudes, and periods can be important in seismic hazard analysis because of the possibility of large earthquakes in the New Madrid region of the Mississippi embayment. In this situation, the AB14mod GMM motions can be a factor of almost 2 greater than the BCA10D GMM motions. Given that the AB14mod attenuation models have $1/\sqrt{R}$ geometric spreading at larger distances, something that almost all models have (e.g., this is true of five of the six attenuation models specified in the NGA-East project, as indicated in table 1.2 of Goulet *et al.*, 2015, the only exception being the BCA10D model), I would judge that they would be the preferred GMMs for long periods and greater distances. Interestingly, the residuals for $T = 2$ s are very similar for all of the GMMs, although those for BCA10D seems to be slightly closer to unity at long periods (Fig. 5).

Taking the above into consideration, I suggest equal weights for the three GMMs. The BCA10D and the AB14mod GMMs are almost end-member representatives in terms of model complexity. The biases and residuals are comparable, but the AB14mod GMMs have a better basis in empirical attenuation studies of Fourier spectra. Giving the two AB14mod GMMs, one-third weights result in the $1/R^{1.3}$ models being given more weight than the $1/R$ model, which I think is appropriate.

The Importance of Path Duration in Comparisons of Models in Terms of PSA versus Distance

Starting with Atkinson (2004), studies of data from small earthquakes seems to support the $1/R^{1.3}$ geometrical spreading at distances within 50 km (although few data are available for distances less than about 10 km; e.g., Atkinson, 2004; Gupta *et al.*, 2017). This would suggest that the AB14mod attenuation models would be preferable to the BCA10D attenuation model at closer distances, as well as at longer distances. But a close look at the study by Gupta *et al.* (2017) suggests that things may be somewhat less transparent. By studying residuals of response spectra (PSA), they find that the Atkinson (2015) empirical model (a model for western North America consistent with $1/R^{1.3}$ geometrical spreading) is in reasonable agreement with data from small-magnitude central and eastern North America earthquakes at distances less than 40 km. Atkinson (2015) found that her empirical model is consistent with simulations in which the path duration (D_P) is given by $0.05R$, but a recent analysis of ENA data by Boore and Thompson (2015) finds a much larger path duration (e.g., 25 s at 50 km rather than 2.5 s from the $D_P = 0.05R$ function). These differences in path duration can make a large difference in the apparent distance attenuation of simulated response spectra. This is shown in Figure 11, which compares PSA at $T = 0.2$ s and **M** 3.5 (approximately the middle of the data used by Gupta

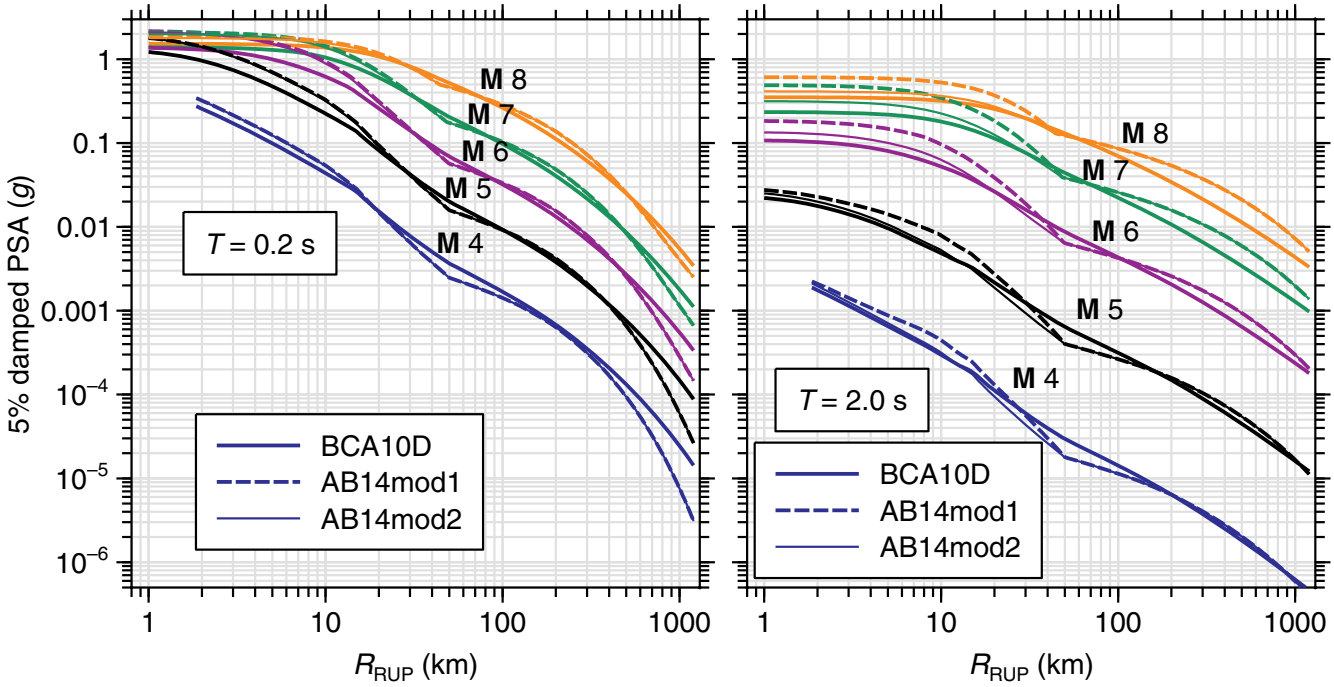

▲ **Figure 6.** Predicted ground motions for periods of (left) 0.2 and (right) 2.0 s for the three recommended attenuation models (and $\Delta\sigma_{200}$). The color version of this figure is available only in the electronic edition.

Table 3
Stress Parameters $\Delta\sigma_{200}$ for Moment Magnitudes M from the NGA-East Flatfile and M Used by Boore (2015; hereafter, B15, Which Are from Boore, 2012), for the BCA10D and the AB14mod1 Attenuation Models (the Results for AB14mod2 Are Not Shown Because They Are Almost Identical to Those from AB14mod1)

Event	Attenuation Model	Description	NGA-East M	$\Delta\sigma_{200}$ (bars)	B15 M	$\Delta\sigma_{200}$ (bars)
Nahanni	BCA10D	−1.0	6.76	60	6.80	57
Saguenay	BCA10D	−1.0	5.85	1353	5.80	1493
Mt. Laurier	BCA10D	−1.0	4.47	296	4.70	160
Cap Rouge	BCA10D	−1.0	4.45	179	4.41	202
St. Anne	BCA10D	−1.0	4.43	161	4.50	134
Kipawa	BCA10D	−1.0	4.62	193	4.70	160
Ausable	BCA10D	−1.0	4.99	156	5.00	153
Riviere-du-Loup	BCA10D	−1.0	4.65	378	4.67	357
Val des Bois	BCA10D	−1.0	5.10	295	5.07	315
Median				**193**		**160**
Nahanni	AB14mod1	−1.0(10)−1.3(50)−0.5	6.76	67	6.80	64
Saguenay	AB14mod1	−1.0(10)−1.3(50)−0.5	5.85	2528	5.80	2809
Mt. Laurier	AB14mod1	−1.0(10)−1.3(50)−0.5	4.47	601	4.70	289
Cap Rouge	AB14mod1	−1.0(10)−1.3(50)−0.5	4.45	340	4.41	393
St. Anne	AB14mod1	−1.0(10)−1.3(50)−0.5	4.43	358	4.50	284
Kipawa	AB14mod1	−1.0(10)−1.3(50)−0.5	4.62	332	4.70	269
Ausable	AB14mod1	−1.0(10)−1.3(50)−0.5	4.99	272	5.00	266
Riviere-du-Loup	AB14mod1	−1.0(10)−1.3(50)−0.5	4.65	846	4.67	788
Val des Bois	AB14mod1	−1.0(10)−1.3(50)−0.5	5.10	631	5.07	679
Median				**358**		**289**

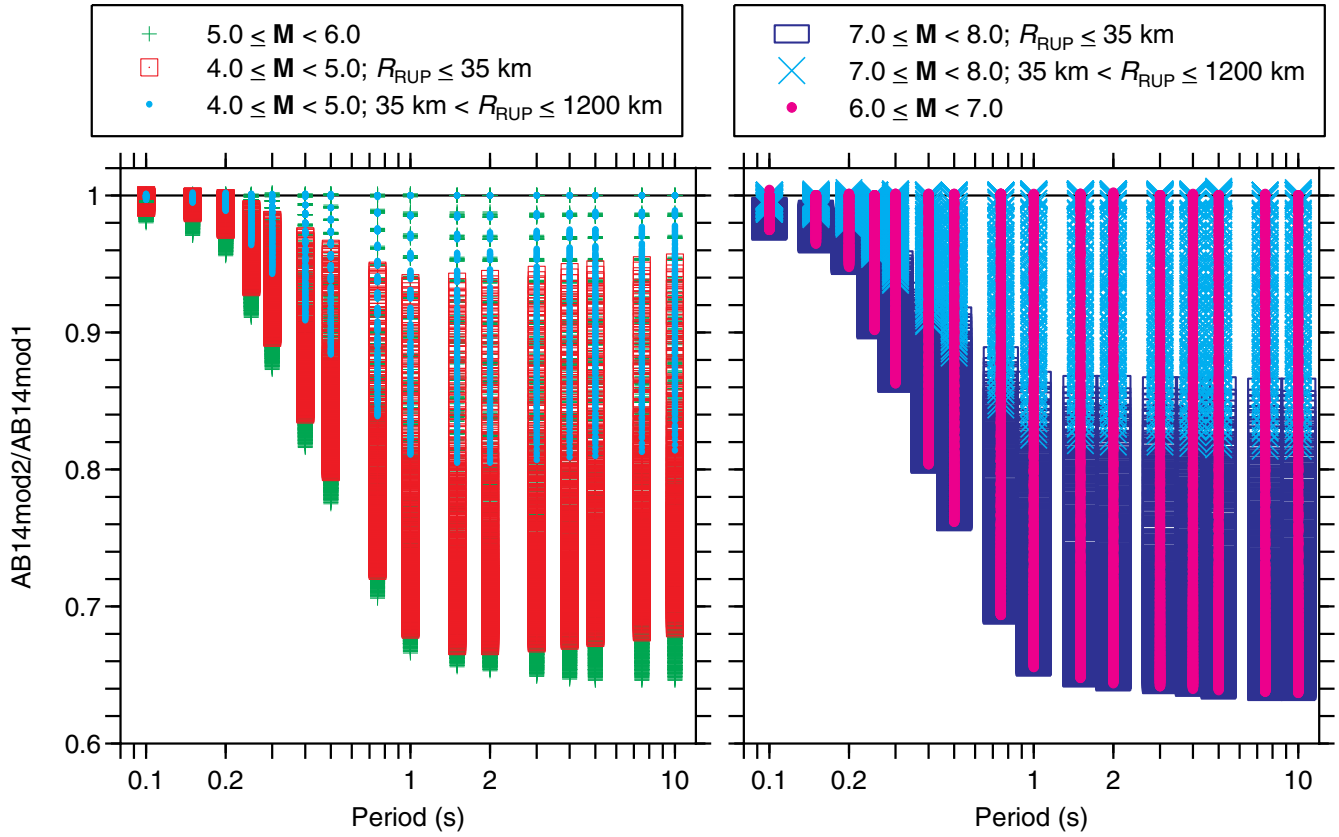

▲ **Figure 7.** Ratio of ground-motion intensity measures (GMIMs) for the AB14mod1 and AB14mod2 GMMs (using the Next Generation Attenuation-East [NGA-East] magnitudes in the determination of the stress parameter). In the grayscale version, what appear to be vertical lines are actually a large number of individual symbols representing various magnitude and distance bins, as follows: small circles, narrow gray line; + and X, medium-width gray line; rectangle, wide dark line. The color version of this figure is available only in the electronic edition.

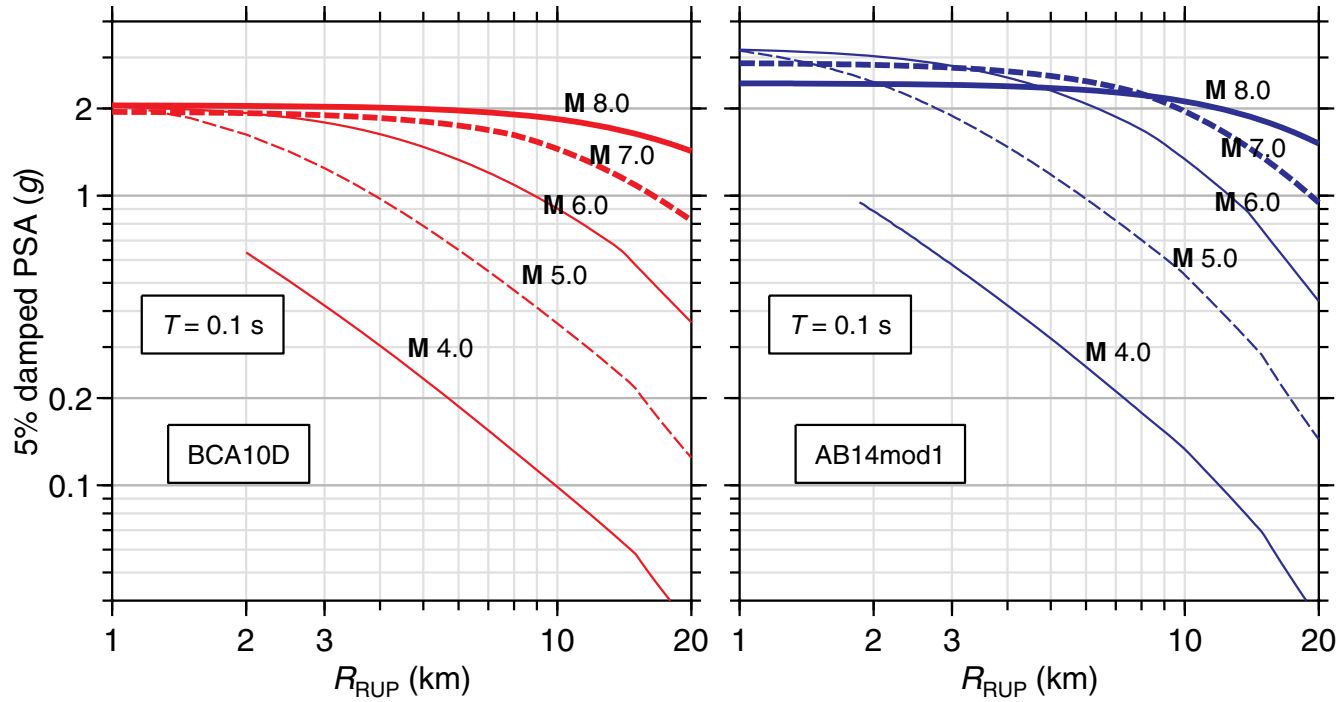

▲ **Figure 8.** PSA for $T = 0.1$ s for short distances, for magnitude ranging from 4.0 to 8.0, for (left) the BCA10D GMM and (right) the AB14mod1 GMM. The color version of this figure is available only in the electronic edition.

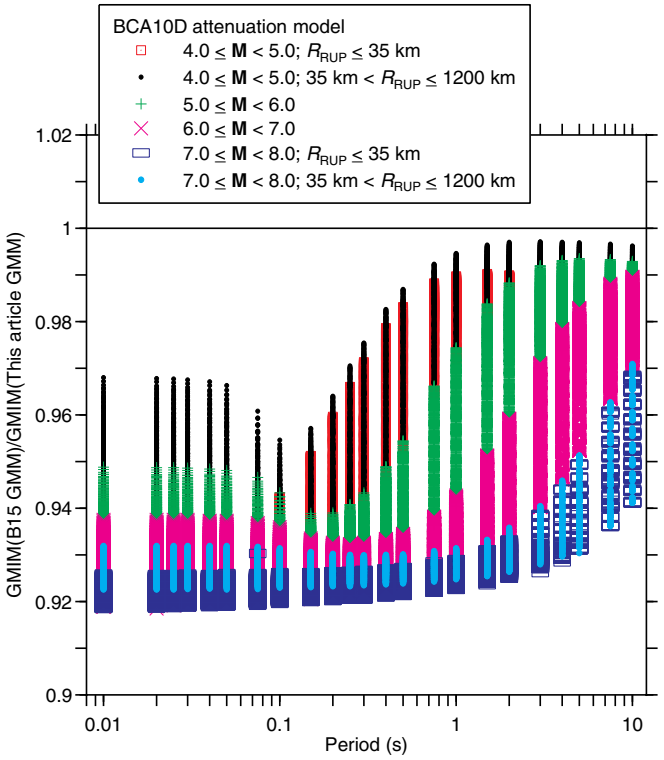

▲ **Figure 9.** Ratio of GMIMs from the BCA10D GMM as provided to NGA-East (Boore, 2015; hereafter, B15) and from this article, as a function of oscillator period. In the grayscale version, what appear to be vertical lines are actually a large number of individual symbols representing various magnitude and distance bins, as follows: small square, medium-width dark line; small dot, narrow-width dark line; +, medium-width light gray line; X, wide dark gray line; rectangle, wide dark line; **M** 7–8, R_{RUP} > 35 km, narrow light gray line. The color version of this figure is available only in the electronic edition.

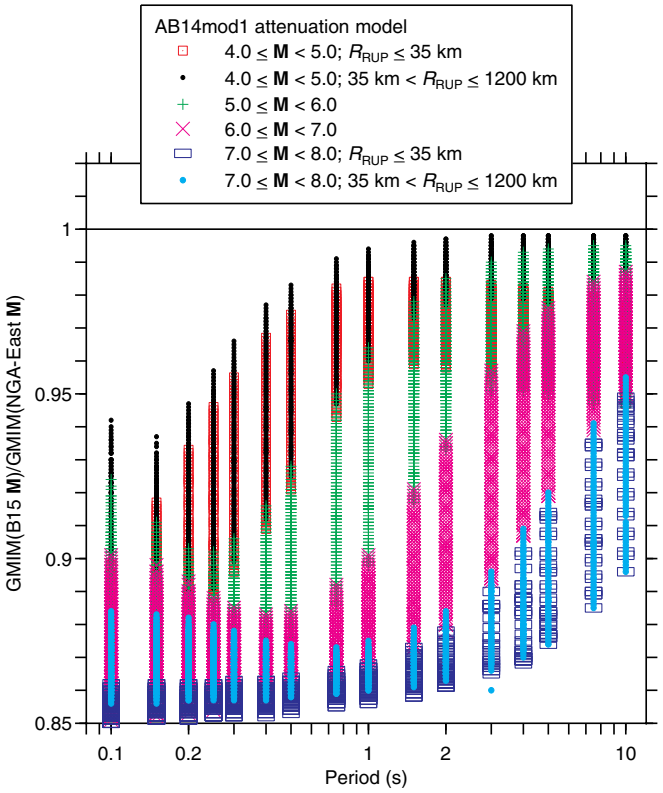

▲ **Figure 10.** Ratio of GMIMs using the B15 magnitudes and the NGA-East magnitudes in the determination of the stress parameter, for the AB14mod1 GMM, as a function of oscillator period. In the grayscale version, what appear to be vertical lines are actually a large number of individual symbols representing various magnitude and distance bins, as follows: small square, medium-width dark line; small dot, narrow-width dark line; +, medium-width light gray line; X, wide dark gray line; rectangle, wide dark line; **M** 7–8, R_{RUP} > 35 km, narrow light gray line. The color version of this figure is available only in the electronic edition.

et al., 2017), computed using the AB14 attenuation model (with $1/R^{1.3}$ spreading within 50 km) and $D_P = 0.05R$ to the PSA using the $1/R$ geometrical spreading of the BCA10D attenuation model and the Boore and Thompson (2015) relation for D_P. The curves have been normalized to the BCA10D curve at 20 km. The decay of response spectra with distance for these very different attenuation models is remarkably similar, demonstrating the importance of D_P in making comparisons of response spectra. A better analysis would be

Table 4
Comparison of Stress Parameters for Moment Magnitudes Used by B15 and from the NGA-East Flatfile, Computed Using the Median of the Stress Parameters for the Nine Individual Events and from the Geometric Mean of the Individual Stress Parameters, but Excluding the Stress Parameter from the Saguenay Earthquake (as Was Done by B15)

Model	M Source	$\Delta\sigma_{200}$ (Using Median) (bars)	$\Delta\sigma_{200}$ (Using Geomean, without Saguenay) (bars)
BCA10D	B15	160	170*
BCA10D	NGA-East	193	190
AB14mod1	B15	289	307
AB14mod1	NGA-East	358	352
AB14mod2	B15	289	309
AB14mod2	NGA-East	358	355

*This differs slightly from the value of 173 bars used by B15 because of minor differences in the inversion procedure.

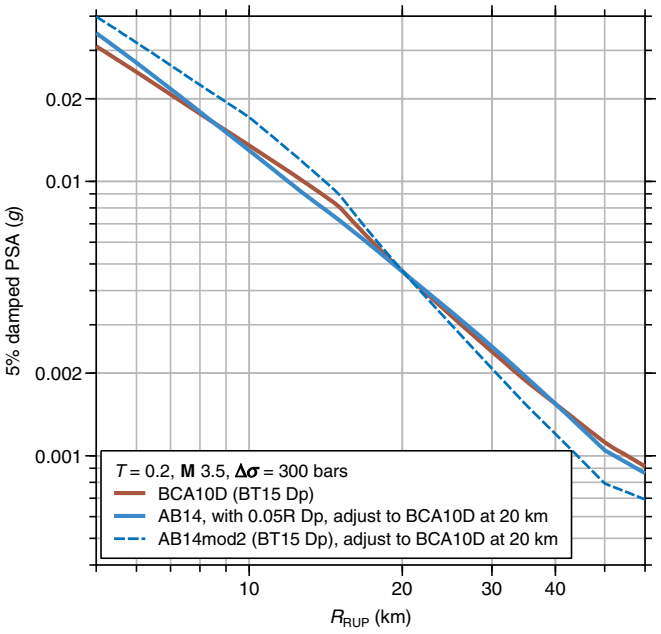

▲ **Figure 11.** Comparison of $T = 0.2$ s PSA from attenuation models with $1/R^{1.3}$ (AB14) and $1/R$ (BCA10D) geometric spreading within 50 km, with the path duration ($D_P = 0.05R_{RUP}$) used by Atkinson (2015) for the $1/R^{1.3}$ model and the Boore and Thompson (2015; referred as BT15) path duration used for the BCA10D model in this article. For comparison, the motions from the AB14mod model used in this article, with $1/R^{1.3}$ geometric spreading from 10 to 50 km, are also shown. The two $1/R^{1.3}$ models have been adjusted to BCA10D at 20 km. The color version of this figure is available only in the electronic edition.

to study the attenuation of Fourier acceleration spectra. This was done by Atkinson and Boore (2014) and, as mentioned earlier, is the main reason for giving more weight to the AB14-mod models than to the BCA10D model.

SUMMARY

The analysis and recommendations for ENA GMMs made for the NGA-East project (Boore, 2015) have been updated by considering three additional models for the attenuation of Fourier spectra and using a mixed-effects analysis of residuals between the predictions from the models and data from nine of the best-recorded larger-magnitude earthquakes for which recordings are available from hard-rock sites in ENA. Based on an analysis of residuals and biases, I recommend three GMMs developed using these attenuation models: BCA10D, with $1/R$ geometrical spreading at all distances, and two modifications of the AB14 model, with $1/R$ spreading within 10 km, $1/R^{1.3}$spreading from 10 to 50 km, and $1/\sqrt{R}$ spreading beyond 50 km. The models are provided as tables, one table per GMIM (peak velocity, peak acceleration, and response spectra for 23 periods). These tables are available in the Ⓔ electronic supplement to this article. The motions in the tables are given for closely spaced magnitudes and distances, and therefore the motions for a particular **M** and R_{RUP} can be easily obtained by interpolation.

What is Missing?

The GMMs are for the median value of the GMIM for very-hard-rock sites (with $V_{S30} = 3000$ m/s, as specified in the NGA-East project, and for $V_{S30} = 2000$ m/s, which is more representative of data from hard-rock sites). The GMMs are provided as tables rather than ground-motion prediction equations (GMPEs). GMPEs might be easier to use than tables, but the NGA-East project required that tables be provided, and tables will be used by the U.S. Geological Survey in making their hazard maps.

For most applications, the GMIMs from the GMMs must be adjusted to site conditions with V_{S30} less than 3000 m/s. This can be done using the results of Stewart *et al.* (2017) and G. A. Parker *et al.* (unpublished report, 2018; see Data and Resources).

Applications for particularly shallow events, such as induced earthquakes, should include adjustments for depth, as discussed in Hollenback *et al.* (2015).

The GMMs specify median ground motions; applications requiring aleatory uncertainties can use the results from other studies, such as Al Atik (2015).

DATA AND RESOURCES

The magnitudes used in the data inversions are from NGA-East_RotD50_5pct_Flatfile_Public_20141118.xlsx (e-Appendix in Goulet *et al.*, 2014). The mixed-effect analysis was done using the linear mixed-effects algorithm (lme function) contained in the nlme package of R (Pinheiro *et al.*, 2017) and available at https://cran.r-project.org/ (last accessed January 2018). The figures were prepared using CoPlot (www.cohort.com, last accessed January 2018). The latest version of the Stochastic-Method SIMulation (SMSIM) programs used for the simulations can be obtained from the online software link at http://www.daveboore.com (last accessed January 2018); their use is described in Boore (2005). The unpublished manuscript by G. A. Parker, J. P. Stewart, Y. M. A. Hashash, E. M. Rathje, K. W. Campbell, and W. J. Silva (2018), "Empirical linear seismic site amplification in central and eastern North America," submitted to *Earthq. Spectra*.

ACKNOWLEDGMENTS

As a result of a conversation with Emrah Yenier, I remembered that I had used the A04QL model in a publication preceding my 2015 Next Generation Attenuation-East (NGA-East) report; for that I thank him. I also thank Linda Al Atik for sending tables from her 2015 Pacific Earthquake Engineering Research Center (PEER) report and Gail Atkinson, Shahram Pezeshk, Valerie Sahakian, Eric Thompson, and Emrah Yenier for comments that improved the article. Any use of trade, firm, or product names is for descriptive purposes only and does not imply endorsement by the U.S. Government.

REFERENCES

Al Atik, L. (2015). NGA-East: Ground motion standard deviation models for Central and Eastern North America, *PEER Report No. 2015/09*, Pacific Earthquake Engineering Research Center, University of California, Berkeley, California, 181 pp.

Atkinson, G. M. (2004). Empirical attenuation of ground-motion spectral amplitudes in southeastern Canada and the northeastern United States, *Bull. Seismol. Soc. Am.* **94,** 1079–1095.

Atkinson, G. M. (2015). Ground-motion prediction equation for small-to-moderate events at short hypocentral distances, with application to induced seismicity hazards, *Bull. Seismol. Soc. Am.* **105,** 981–992.

Atkinson, G. M., and K. Assatourians (2010). Attenuation and source characteristics of the 23 June 2010 M 5.0 Val-des-Bois, Quebec, earthquake, *Seismol. Res. Lett.* **81,** 849–860.

Atkinson, G. M., and D. M. Boore (1995). Ground motion relations for eastern North America, *Bull. Seismol. Soc. Am.* **85,** 17–30.

Atkinson, G. M., and D. M. Boore (2006). Earthquake ground-motion prediction equations for eastern North America, *Bull. Seismol. Soc. Am.* **96,** 2181–2205.

Atkinson, G. M., and D. M. Boore (2014). The attenuation of Fourier amplitudes for rock sites in eastern North America, *Bull. Seismol. Soc. Am.* **104,** 513–528.

Atkinson, G. M., J. Hollenback, and R. W. Graves (2015). Selection of attenuation models, appendix 1A in chapter 1 of NGA-East: Median ground-motion models for the Central and Eastern North America region, *PEER Report 2015/04*, Pacific Earthquake Engineering Research Center, Berkeley, California.

Boatwright, J., and L. Seekins (2011). Regional spectral analysis of three moderate earthquakes in northeastern North America, *Bull. Seismol. Soc. Am.* **101,** 1769–1782.

Boore, D. M. (2003). Prediction of ground motion using the stochastic method, *Pure Appl. Geophys.* **160,** 635–676.

Boore, D. M. (2005). SMSIM—Fortran programs for simulating ground motions from earthquakes: Version 2.3—A revision of OFR 96-80-A, U.S. Geological Survey Open-File Report, *U. S. Geol. Surv. Open-File Rept. 00-509*, revised 15 August 2005, 55 pp.

Boore, D. M. (2012). Updated determination of stress parameters for nine well-recorded earthquakes in eastern North America, *Seismol. Res. Lett.* **83,** 190–199.

Boore, D. M. (2015). Point-source stochastic-method simulations of ground motions for the PEER NGA-East project, chapter 2 in NGA-East: Median ground-motion models for the Central and Eastern North America region, *PEER Report 2015/04*, Pacific Earthquake Engineering Research Center, Berkeley, California, 11–49.

Boore, D. M., and E. M. Thompson (2015). Revisions to some parameters used in stochastic-method simulations of ground motion, *Bull. Seismol. Soc. Am.* **105,** 1029–1041.

Boore, D. M., K. W. Campbell, and G. M. Atkinson (2010). Determination of stress parameters for eight well-recorded earthquakes in eastern North America, *Bull. Seismol. Soc. Am.* **100,** 1632–1645.

Boore, D. M., J. P. Stewart, E. Seyhan, and G. M. Atkinson (2014). NGA-West2 equations for predicting PGA, PGV, and 5%-damped PSA for shallow crustal earthquakes, *Earthq. Spectra* **30,** 1057–1085.

Chapman, M. C., and R. W. Godbee (2012). Modeling geometrical spreading and the relative amplitudes of vertical and horizontal high-frequency ground motions in eastern North America, *Bull. Seismol. Soc. Am.* **102,** 1957–1975.

Frankel, A. (2015). Decay of S-wave amplitudes with distance for earthquakes in the Charlevoix, Quebec, area: Effects of radiation pattern and directivity, *Bull. Seismol. Soc. Am.* **105,** 850–857.

Goulet, C. A., Y. Bozorgnia, and N. A. Abrahamson (2015). Introduction, chapter 1 in NGA-East: Median ground-motion models for the Central and Eastern North America region, *PEER Report 2015/04*, Pacific Earthquake Engineering Research Center, Berkeley, California, 11–49.

Goulet, C. A., Y. Bozorgnia, N. Kuehn, L. Al Atik, R. R. Youngs, R. W. Graves, and G. M. Atkinson (2017). NGA-East ground-motion models for the U.S. Geological Survey National Seismic Hazard Maps, *PEER Report 2017/03*, Pacific Earthquake Engineering Research Center, Berkeley, California, 163 pp.

Goulet, C. A., T. Kishida, T. D. Ancheta, C. H. Cramer, R. B. Darragh, W. J. Silva, Y. M. A. Hashash, J. Harmon, J. P. Stewart, K. E. Wooddell, *et al.* (2014). PEER NGA-East database, *PEER Report 2014/17*, Pacific Earthquake Engineering Research Center, Berkeley, California, 97 pp.

Gupta, A., J. W. Baker, and W. L. Ellsworth (2017). Assessing ground-motion amplitudes and attenuation for small-to-moderate induced and tectonic earthquakes in the central and eastern United States, *Seismol. Res. Lett.* **88,** 1379–1389.

Hollenback, J., C. A. Goulet, and D. M. Boore (2015). Adjustment for source depth, chapter 3 in NGA-East: Adjustments to median ground-motion models for Central and Eastern North America, *PEER Report 2015/08*, Pacific Earthquake Engineering Research Center, Berkeley, California, 31–66.

Kale, Ö., and S. Akkar (2013). A New procedure for selecting and ranking ground-motion prediction equations (GMPEs): The Euclidean distance-based ranking (EDR) method, *Bull. Seismol. Soc. Am.* **103,** 1069–1084.

Mak, S., R. A. Clements, and D. Schorlemmer (2017). Empirical evaluation of hierarchical ground motion models: Score uncertainty and model weighting, *Bull. Seismol. Soc. Am.* **107,** 949–965.

Pinheiro, J., D. Bates, S. DebRoy, D. Sarkar, and R Core Team (2017). nlme: Linear and nonlinear mixed effects models. R package version 3.1-131, available at https://CRAN.R-project.org/package=nlme (last accessed January 2018).

Scasserra, G., J. P. Stewart, P. Bazzurro, G. Lanzo, and F. Mollaioli (2009). A comparison of NGA ground-motion prediction equations to Italian data, *Bull. Seismol. Soc. Am.* **99,** 2961–2978.

Scherbaum, F., E. Delavaud, and C. Riggelsen (2009). Model selection in seismic hazard analysis: An information-theoretic perspective, *Bull. Seismol. Soc. Am.* **99,** 3234–3247.

Sedaghati, F., and S. Pezeshk (2016). Estimation of the coda-wave attenuation and geometrical spreading in the New Madrid seismic zone, *Bull. Seismol. Soc. Am.* **106,** 1482–1498.

Silva, W., N. Gregor, and R. Darragh (2002). Development of hard rock attenuation relations for central and eastern North America, internal report, Pacific Engineering, November 1, 2002, available at http://pacificengineering.org/CEUS/Development%20of%20Regional%20Hard_ABC.pdf (last accessed January 2018).

Stewart, J. P., G. A. Parker, J. A. Harmon, G. M. Atkinson, D. M. Boore, R. B. Darragh, W. J. Silva, and Y. M. A. Hashash (2017). Expert panel recommendations for ergodic site amplification in Central and Eastern North America, *PEER 2017/03*, Pacific Earthquake Engineering Research Center, University of California, Berkeley, California, 51 pp.

Wu, Q., M. C. Chapman, J. N. Beale, and S. Shamsalsadati (2016). Near-source geometrical spreading in the central Virginia seismic zone determined from the aftershocks of the 2011 Mineral, Virginia, earthquake, *Bull. Seismol. Soc. Am.* **106,** 943–955.

Youngs, R. R., and N. Kuehn (2015). Extension of median ground-motion models to short and large distances, chapter 2 in NGA-East: Adjustments to median ground-motion models for Central and Eastern North America, *PEER Report 2015/08*, Pacific Earthquake Engineering Research Center, University of California, Berkeley, California, 9–29.

David M. Boore
U.S. Geological Survey
345 Middlefield Road, Mail Stop 977
Menlo Park, California 94025 U.S.A.
boore@usgs.gov

Published Online 21 February 2018